REGULAR ARTICLE

blood advances

Genome-wide screening identifies cell-cycle control as a synthetic lethal pathway with SRSF2^{P95H} mutation

Jane Jialu Xu,[1,2] Alistair M. Chalk,[1,2] Iva Nikolic,[3,4] Kaylene J. Simpson,[3,4] Monique F. Smeets,[1,2,*] and Carl R. Walkley[1,2,5,*]

[1]St Vincent's Institute, Fitzroy, VIC, Australia; [2]Department of Medicine, St Vincent's Hospital, University of Melbourne, Fitzroy, VIC, Australia; [3]Victorian Centre for Functional Genomics, Peter MacCallum Cancer Centre, Victorian Comprehensive Cancer Centre, Parkville, VIC, Australia; [4]Sir Peter MacCallum Department of Oncology, University of Melbourne, Parkville, VIC, Australia; and [5]Mary MacKillop Institute for Health Research, Australian Catholic University, Melbourne, VIC, Australia

Key Points

- Disruption of cell-cycle control and DNA damage response pathways are synthetic lethal with *Srsf2*$^{P95H/+}$.
- Palbociclib preferentially targets *Srsf2*$^{P95H/+}$ cells.

Current strategies to target RNA splicing mutant myeloid cancers proposes targeting the remaining splicing apparatus. This approach has only been modestly sensitizing and is also toxic to non-mutant-bearing wild-type cells. To explore potentially exploitable genetic interactions with spliceosome mutations, we combined data mining and functional screening for synthetic lethal interactions with an *Srsf2*$^{P95H/+}$ mutation. Analysis of missplicing events in a series of both human and murine *SRSF2*^{P95H} mutant samples across multiple myeloid diseases (acute myeloid leukemia, myelodysplastic syndromes, chronic myelomonocytic leukemia) was performed to identify conserved missplicing events. From this analysis, we identified that the cell-cycle and DNA repair pathways were overrepresented within the conserved misspliced transcript sets. In parallel, to functionally define pathways essential for survival and proliferation of *Srsf2*$^{P95H/+}$ cells, we performed a genome-wide Clustered regularly interspaced short palindromic repeat loss-of-function screen using Hoxb8 immortalized *R26*-CreER$^{ki/+}$ *Srsf2*$^{P95H/+}$ and *R26*-CreER$^{ki/+}$ *Srsf2*$^{+/+}$ cell lines. We assessed loss of single guide RNA representation at 3 timepoints: immediately after *Srsf2*$^{P95H/+}$ activation, and at 1 week and 2 weeks after *Srsf2*$^{P95H/+}$ mutation. Pathway analysis demonstrated that the cell-cycle and DNA damage response pathways were among the top synthetic lethal pathways with *Srsf2*$^{P95H/+}$ mutation. Based on the loss of guide RNAs targeting *Cdk6*, we identified that palbociclib, a CDK6 inhibitor, showed preferential sensitivity in *Srsf2*$^{P95H/+}$ cell lines and in primary nonimmortalized lin$^-$cKIT$^+$Sca-1$^+$ cells compared with wild-type controls. Our data strongly suggest that the cell-cycle and DNA damage response pathways are required for *Srsf2*$^{P95H/+}$ cell survival, and that palbociclib could be an alternative therapeutic option for targeting *SRSF2* mutant cancers.

Introduction

Mutations in the core RNA splicing machinery (termed the spliceosome) have been identified as 1 of the most frequently mutated pathways in myeloid neoplasms.[1] There is increasing evidence linking specific mutations in the spliceosome with distinct phenotypic and clinical outcomes. The RNA splicing factor SRSF2 is mutated in 11% to 15% of myelodysplastic syndromes (MDS) and 28% to 47% of chronic myelomonocytic leukemia.[2] Mutations in *SRSF2* cluster at or around proline 95, with proline to histidine

Submitted 22 February 2021; accepted 4 May 2021; prepublished online on *Blood Advances* First Edition 31 August 2021; final version published online 30 March 2022. DOI 10.1182/bloodadvances.2021004571.

*M.F.S. and C.R.W. contributed equally to this work.

All datasets related to this work are deposited in GEO (GSE165506).

The full-text version of this article contains a data supplement.

(P95H) being the most common mutation. SRSF2^{P95H} has been shown to lead to altered recognition of binding motifs on the exonic splicing enhancer, resulting in aberrantly spliced transcripts.[3,4] So far, various groups have attempted to decipher the link between SRSF2^{P95H}-specific missplicing events and MDS pathogenesis. Despite identification of recurrently misspliced transcripts, such as *HNRNPA2B1* and *FYN*, it remains unclear how the spliceosome mutations and the resultant misspliced transcripts contribute to the initiation and development of MDS and related myeloid neoplasms.[3-5]

In parallel to understanding the effect of splicing factor mutations on hematopoiesis, therapies targeting splicing mutations have been proposed. Spliceosome mutations are nearly always heterozygous and mutually exclusive, which suggests that the remaining wild-type (WT) allele in the mutant cells is crucial for maintaining a level of splicing necessary for cell survival.[6-8] Small molecule spliceosome inhibitors, such as Pladienolide B, E7107, Spliceostatin A, and H3B-8800, interfere with the binding of SF3B1 and cause cell-cycle arrest in splicing mutant cells.[9-11] However, 2 phase 1 clinical trials (NCT00459823, NCT00499499) observed unexpected ophthalmic adverse effects with spliceosome inhibitors E7107.[12] A preliminary report of a recent phase 1 clinical trial of H3B-8800 (NCT02841540) indicates that the compound failed to induce complete or partial clinical response in patients with acute myeloid leukemia, MDS, and chronic myelomonocytic leukemia.[13] The lack of effective treatments for MDS and related myeloid cancers and the high prevalence of spliceosomal mutations highlights the need to explore the therapeutic targeting of splicing mutant cells without disruption of splicing catalysis.

An attractive therapeutic strategy for cancer is the identification of synthetic lethal interactions, exemplified by the use of PARP inhibitors in *BRCA*-mutated cancers.[14] A synthetic lethal interaction involves 2 genes in which mutation of either one is viable, but perturbation of both genes simultaneously is lethal to the cell.[15] Thus, it provides opportunities to advance specific anticancer therapies, especially when the driver mutation is not readily druggable.[16] From RNA interference screens in yeast to Clustered regularly interspaced short palindromic repeats (CRISPR) screens in mammalian in vivo systems, larger scale and more clinically relevant models have been developed and have identified new targets in their respective cancers settings.[17] These approaches are now widely applicable with the availability of genetic perturbation tools and the development of inducible, physiologically expressed mutations found in human cancers in both human cell lines and in murine models.

Here, we report a pooled in vitro CRISPR loss of function screen to decipher the genetic vulnerabilities of *Srsf2*$^{P95H/+}$ cells. We have made use of cell lines derived from our genetically engineered conditional knock-in model of *Srsf2*$^{P95H/+}$ mutation.[18,19] This model recapitulates the core characteristics of human disease associated with *SRSF2* mutation and develops an MDS/myeloproliferative neoplasm phenotype in vivo. Using this unbiased whole genome approach, we identified that cell-cycle control and DNA damage response pathways play an important role in the survival of *Srsf2*$^{P95H/+}$ cells. By overlaying the genetic interactors with the drug–gene interaction database, we identified that the CDK6 inhibitor palbociclib could preferentially target the *Srsf2*$^{P95H/+}$ mutant cells. Collectively, these results demonstrate that there are potentially exploitable genetic vulnerabilities in *Srsf2*$^{P95H/+}$ mutant cells outside of the RNA splicing machinery.

Methods

Mice

All mouse experiments were approved by the Animal Ethics Committee, St. Vincent's Hospital, Melbourne, Australia (AEC#001/16 and 007/19). Mice used in the experiments were housed at the Bio-Resource Centre located at St. Vincent's Hospital. *Rosa26*-CreER^{T2} *Srsf2*$^{P95H/+}$ mice have been previously described.[18]

DNA isolation and genotyping

Genomic DNA was extracted from cell pellets using a Bioline Genomic DNA kit as per manufacturer's instructions. Genotyping was performed by polymerase chain reaction (PCR) in the Mastercycler Pro PCR machine (Eppendorf). The oligonucleotides (IDT, Singapore) used for Srsf2 P95H genotyping PCR are:

SRSF2 5'loxP forward primer: 5'-GTTATGATCCACACCTCT-CACC-3';

SRSF2 5'loxP reverse primer: 5'-ATAAACGTTTATGTCCGCTACC-3'.

Product size: WT = 327 bp; recombined = 400 bp; 5'loxP (floxed) intact = 446 bp.

Generation of Hoxb8 immortalized and Cas9 expressing cell lines

Hoxb8 immortalized cell lines. Briefly, Ficoll separated bone marrow cells from 3 *R26*-CreER^{T2} *Srsf2*$^{P95H/+}$ and 3 *R26*-CreER^{T2} *Srsf2*$^{+/+}$ mice, were stimulated for 48 hours in complete Iscove modified Dulbecco medium (IMDM [Sigma Aldrich] containing 20% fetal bovine serum [FBS, Assay Matrix], 1% penicillin/streptomycin [Gibco], 1% glutamine [Gibco]) supplemented with recombinant mouse stem cell factor (50 ng/mL, PeproTech), recombinant mouse interleukin-3 (10 ng/mL, PeproTech), and recombinant human interleukin-6 (10 ng/mL, Amgen). After stimulation, 1×10^6 cells were spin-infected with Hoxb8 retrovirus[20] (Hoxb8 plasmids were generously provided by Mark Kamps, University of California San Diego) and polybrene at 1100*g* for 90 minutes. After 48 hours, cells were then passaged into complete IMDM containing 1% granulocyte-macrophage colony-stimulating factor (GM-CSF) conditioned medium (from BHK-HM5 cell conditioned medium).

Cas9 expressing cell lines. Hoxb8 immortalized cell lines were infected with Cas9-blasticidin lentivirus (lentiCas9-Blast was a gift from Feng Zhang; Addgene plasmid #52962)[21] by spin infection at 1100*g* for 90 minutes. The infected cells were then cultured in IMDM-Cas9 medium (IMDM, 10% FBS, 1% GM-CSF, and 3 μg/mL blasticidin) for 2 weeks to select for a Cas9-expressing population.

Srsf2$^{P95H/+}$ CRISPR knockout pooled library screen

See supplemental Methods for full method description.

CRISPR screen sample preparation and sgRNA library sequencing

Genomic DNA was extracted from the cell pellets using the Gentra Puregene kit (Qiagen). The extracted DNA was quantified on a

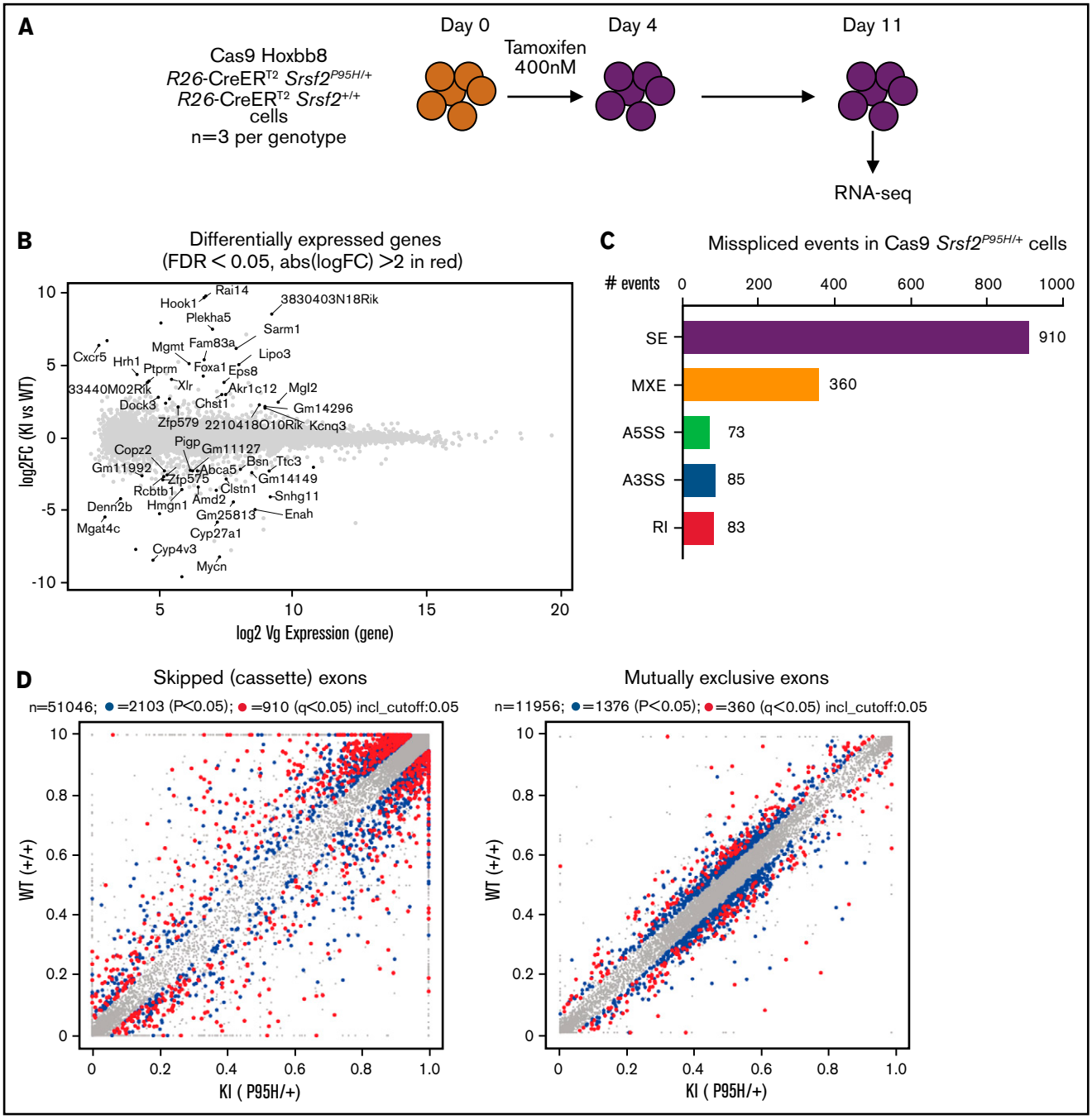

Figure 1. Cas9 *Srsf2*$^{P95H/+}$ cell lines show similar missplicing changes as primary cells. (A) A schematic diagram depicting the experimental design for RNA sequencing. (B) An MA plot showing differentially expressed genes in the *Srsf2*$^{P95H/+}$ cells compared with *Srsf2*$^{+/+}$; red dots = FDR < .05, absolute fold change >2, genes without symbols are not labeled. (C) The number of misspliced events in GM-CSF *Srsf2*$^{P95H/+}$ cells. A3SS alternative 3' splicing site; A5SS, alternative 5' splicing site; MXE, mutually exclusive exon; RI, retained intron; SE, skipped exon. (D) Scatter plots of the GM-CSF *Srsf2*$^{P95H/+}$ cells showing the skipped (cassette) exons and mutually exclusive exon events. Gray dots, <5% difference between genotypes; blue dots, $P < .05$ and >5% difference between genotypes; red dots, $q < .05$ and >5% difference between genotypes. (E) Sashimi plot of selected missplicing events in the myeloid cell lines.

Nanodrop spectrophotometer. DNA libraries were generated by PCR amplification of the integrated single guide RNA (sgRNA) constructs (as described at https://portals.broadinstitute.org/gpp/public/resources/protocols). In total, 24 libraries were generated and sequenced on the Illumina platform using 150-bp paired end reads by Novogene (China). CRISPR screen analysis was performed using MaGeCK, MaGeCK-VISPR, and the CRISPRBetaBinomial package (v1.3.0).[22-24] The heatmap for negatively selected pathway analysis was generated with Metascape.[25]

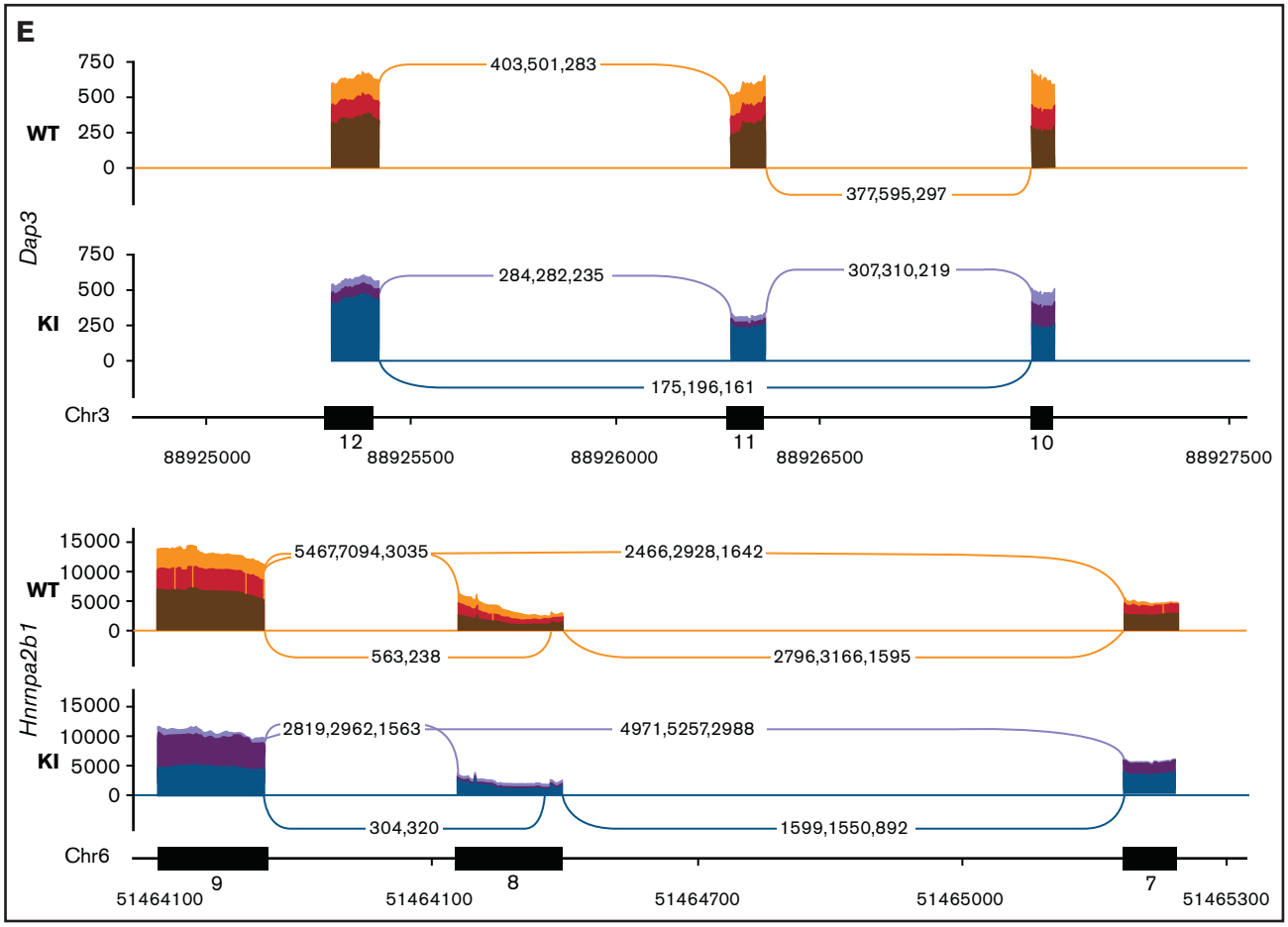

Figure 1. (continued)

RNA-sequencing

RNA was isolated from Cas9 *R26*-CreER^{T2} *Srsf2*$^{P95H/+}$ and *R26*-CreER^{T2} *Srsf2*$^{+/+}$ cells (n = 3 per genotype) at 7 days after tamoxifen treatment. RNA was ribosome depleted, subjected to library preparation (Kapa Stranded RNA-Seq Library Kit; Kapa Biosystems),[18,26,27] and sequenced at 150-bp paired-end reads on the Illumina platform by Novogene (China). Differential expression was assessed using DESeq2.[28] Splicing analysis was performed using rMATs as described previously.[18] Alternative splicing analysis was performed using PSI-Sigma (v1.9) using nreads = 5.[29] The Sashimi plots were generated using ggSashimi.[30]

Palbociclib sensitivity assay

Hoxb8 *R26*-CreER^{T2} *Srsf2*$^{P95H/+}$ and *R26*-CreER^{T2} *Srsf2*$^{+/+}$ cell lines were treated with 400 nM 4-hydroxy tamoxifen for 4 days. At 48 hours after tamoxifen cessation, 1000 cells were plated in 50 μL of IMDM with 10% FBS and 1% GM-CSF in a 96-well tissue culture plate and 50 μL of a 2× concentration of drugs was added in triplicate per dose. For the lin-c-Kit$^+$Sca-1$^+$ (LKS$^+$) in vitro drug assay, sorted LKS$^+$ cells were cultured for 24 hours in cytokine-supplemented complete IMDM (20% FBS, 50 ng/mL recombinant mouse stem cell factor, 10 ng/mL recombinant mouse interleukin-3, 10 ng/mL recombinant human interleukin-6), and then treated with 400 nM 4-hydroxy tamoxifen for 4 days. The treated LKS$^+$ cells were then plated for drug assays as described previously. A dimethyl sulfoxide or water control was included in all assays. Cell viability was assessed after 4 days of drug culture using the ATP-Lite Luminescence Assay System (Perkin Elmer) and an Enspire plate reader (Perkin Elmer). The 50% inhibitory concentration (IC_{50}) was calculated in Prism 8 (GraphPad) using log(inhibitor) vs normalized response-variable slope. Statistical analysis was performed with extra sum-of-squares F test. $P < .05$ is considered as significant.

Results

Cas9 *Srsf2*$^{P95H/+}$ cell lines have similar splicing changes as primary cells from the in vivo models

To obtain a cell line model suitable for genome-wide CRISPR knock-out screening, we generated Hoxb8 immortalized myeloid cell lines from the bone marrow of 3 *R26*-CreER^{T2} *Srsf2*$^{P95H/+}$ and 3 *R26*-CreER^{T2} *Srsf2*$^{+/+}$ mice[18] (supplemental Figure 1). These were then engineered to express Cas9. To determine if the Cas9 expressing Hoxb8 *Rosa26*-CreER$^{T2ki/+}$ *Srsf2*$^{P95H/+}$ cells (referred to as Cas9 *Srsf2*$^{P95H/+}$ cells) had splicing changes similar to primary *Srsf2*$^{P95H/+}$ cells,[18] we tamoxifen-treated the Cas9 *Srsf2*$^{P95H/+}$ and Cas9 *Srsf2*$^{+/+}$ cells (n = 3 per genotype) to

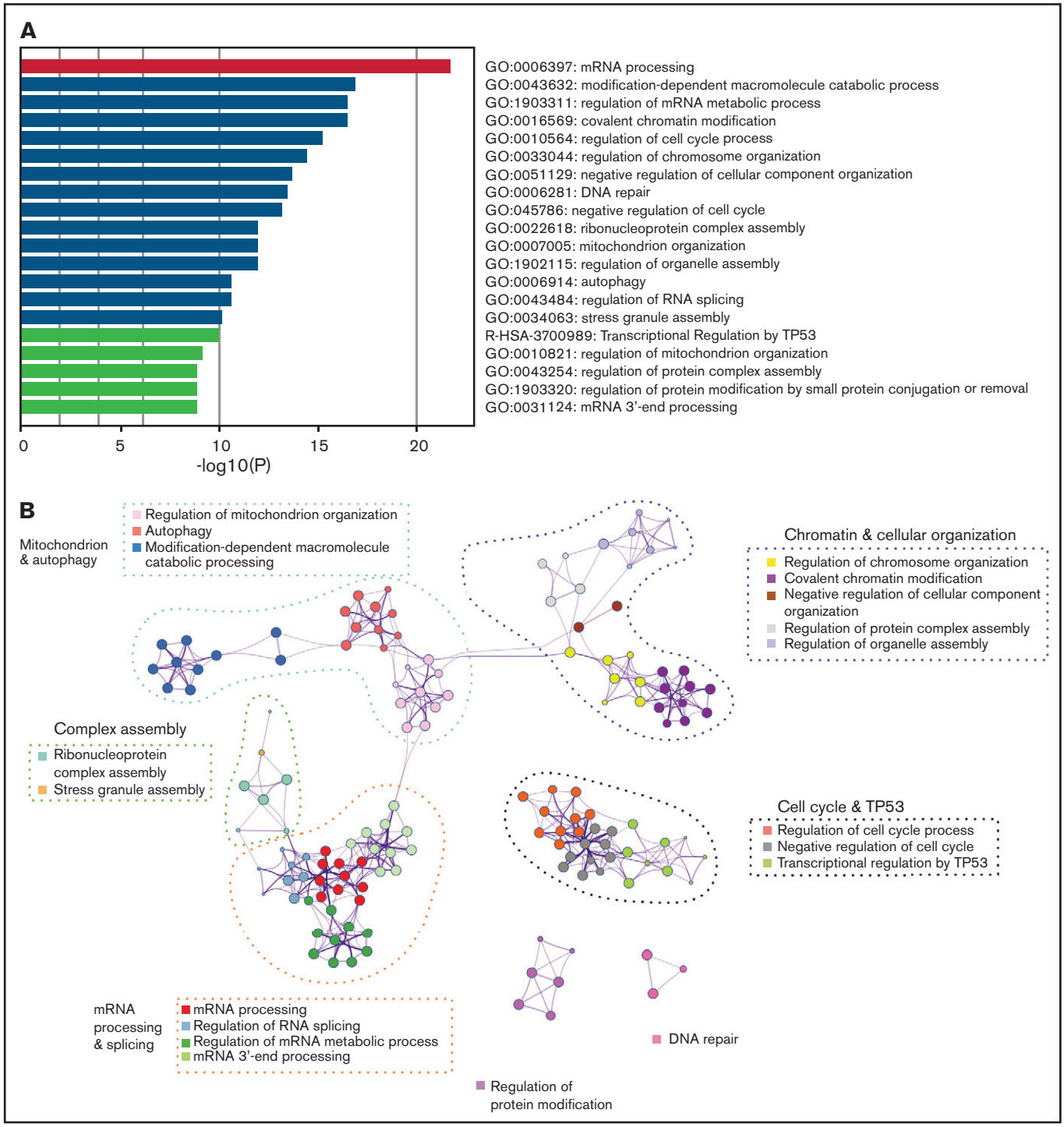

Figure 2. Common misspliced pathways in 16 *Srsf2/SRSF2* mutant cells. (A) The pathways most frequently represented within the misspliced transcript sets in the *Srsf2/SRSF2* mutant cells. (B) Protein–protein interaction networks between the common transcripts misspliced in *Srsf2/SRSF2* mutant cells.

activate the mutation and performed RNA-sequencing (RNA-seq) on cells at 7 days after tamoxifen treatment (Figure 1A). At this time point, there were a limited number of differentially expressed transcripts detected between the Cas9 *Srsf2*$^{P95H/+}$ and *Srsf2*$^{+/+}$ cells (Figure 1B; supplemental Figure 2). Using rMATS[31] to identify differential alternative splicing events, we found that in the *Srsf2*$^{P95H/+}$ cells skipped exons (n = 910) were the most frequent type of altered splicing, followed by mutually exclusive exons (n = 360), alternative 5' splice sites (n = 73), alternative 3' splice sites (n = 85), and retained introns (n = 83) (Figure 1C). We used an inclusion cutoff of 0.05 to identify changes in splicing, meaning that to be included in the analysis, exons were required to be at least 5% differentially spliced. At a false discovery rate (FDR) of 5%, less than 2% of the total events were significantly different for skipped

Table 1. Genes identified as misspliced in *Srsf2/SRSF2* mutant cells in at least 10 of 16 datasets

Gene	Description	No. of datasets (human/murine)
ATF2	Activating transcription factor 2	13 (7H/6M)
MTMR14	Myotubularin related protein 14	13 (9H/4M)
HNRNPA2B1	Heterogenous nuclear ribonucleoprotein A2/B1	11 (5H/6M)
SEC24B	SEC24 family member B	11 (6H/5M)
AGTPBP1	ATP/GTP binding protein 1	10 (5H/5M)
PRPSAP2	Phosphoribosyl pyrophosphate synthetase-associated protein 2	10 (6H/4M)
EHMT2	Euchromatic histone-lysine *N*-methyltransferase 2	10 (5H/5M)
STRADA	STE20-related kinase adaptor α	10 (5H/5M)
TIA1	TIA1 cytotoxic granule-associated RNA binding protein	10 (5H/5M)
MTF2	Metal response element binding transcription factor 2	10 (5H/5M)
RSRC2	Arginine/serine-rich coiled-coil 2	10 (7H/3M)
CEP57	Centrosomal protein 57kDa	10 (8H/2M)
FIP1L1	Factor interacting with PAPOLA and CPSF1	10 (7H/3M)
FYN	FYN proto-oncogene, Src family tyrosine kinase	10 (6H/4M)
ABI1	Abl-interactor 1	10 (6H/4M)
HUWE1	HECT, UBA, and WWE domain containing 1, E3 ubiquitin protein ligase	10 (5H/5M)
TPD52L2	Tumor protein D52-like 2	10 (8H/2M)
ZMYND8	Zinc finger, MYND-type containing 8	10 (7H/3M)
NSD1	Nuclear receptor binding SET domain protein 1	10 (5H/5M)

Genes are ranked by the number of datasets the transcript was identified in. The number of human (H) or murine (M) datasets is indicated in parentheses.

exons and 3% of total events were significantly different for mutually exclusive exons (Figure 1D). The magnitude of splicing changes observed in Cas9 *Srsf2*$^{P95H/+}$ cells was therefore similar to other SRSF2^{P95H} mutant cell lines, as well as in vivo models.[3,5,18] We then assessed specific genes that were reported previously, including from our and other studies. Indeed, previously identified misspliced targets of *Srsf2*$^{P95H/+}$ such as *Dap3* and *Hnrnpa2b1*, were aberrantly spliced in the Cas9 *Srsf2*$^{P95H/+}$ cells (Figure 1E).[4,5,18] These data demonstrate that the Cas9 *Srsf2*$^{P95H/+}$ cells are recapitulating changes in splicing observed in primary cells and represent a tractable system to further study the effect of *Srsf2* mutation in vitro, without the interference of other cooccurring mutations in myeloid leukemia.

Cell-cycle regulation and DNA repair pathways are overrepresented within the misspliced transcript set of *SRSF2* mutant cells

To understand the landscape of missplicing in *SRSF2* mutated cells, we literature-curated misspliced genes from 16 different human and murine datasets of *SRSF2* mutation, including the Cas9 *Srsf2* cells described previously (supplemental Table 1).[3-5,18,32-36] Metascape pathway enrichment analysis was performed on genes that were identified in more than 4 of the 16 datasets, regardless of the type of misspliced event.[25] This analysis revealed that in *SRSF2* mutant cells, messenger RNA (mRNA) processing was the most frequently overrepresented pathway of the top 20 pathways that were most significantly enriched for misspliced transcripts (Figure 2A). In the network map of enriched pathways, pathways associated with regulation of the cell cycle, chromatin and cellular organization, mitochondrion, complex assembly, DNA repair, and protein modification were also identified (Figure 2B). Individual genes identified as having altered splicing in 10 of 16 datasets are listed in Table 1. This includes known targets of SRSF2^{P95H}, such as *HNRNPA2B1* and *FYN*, as well as genes such as *ATF2*, which has been shown to be involved in cell-cycle and DNA repair regulation.[37,38]

Selection of MDS related genes in *Srsf2* mutant cells mirrors human genetic interactions

In parallel to the literature analysis, we performed a genome-wide pooled CRISPR knock-out screen using the Cas9 expressing cells to explore the genetic vulnerabilities induced by *Srsf2*^{P95H} mutation (Figure 3A). Cas9 *Srsf2*$^{P95H/+}$ or Cas9 *Srsf2*$^{+/+}$ cells (n = 3 biological replicates per genotype) were transduced with the Brie sgRNA library, which targets 19c674 genes with 4 sgRNAs per gene.[39] After selection for cells infected with the sgRNA library with puromycin, the cells were used for screening. At day 0 of the screen, cells expressing sgRNAs were treated with tamoxifen (400 nM) for 4 days to activate expression of the *Srsf2*$^{P95H/+}$ mutation. Cells were then cultured for up to 14 days after tamoxifen treatment. Genomic DNA from each cell line was collected at days 0, 4, 11, and 18 and sequenced to determine the sgRNA representation compared with the baseline (day 0) sgRNA counts (outlined in Figure 3A).

Analysis of sgRNA counts was performed with both CRISPRBeta-Binomial and MaGeCK VISPR.[22,23] The number of mapped reads per sample ranged from 24 to 33 million, with an average mappability of 85%. The average copy number of the sgRNAs was 355 (supplemental Table 2) and was equally distributed across the cell lines, suggesting equivalent sgRNA representation across samples (supplemental Table 3A). As expected, the diversity of the sgRNA pool decreased over time (supplemental Table 3B). The correlation

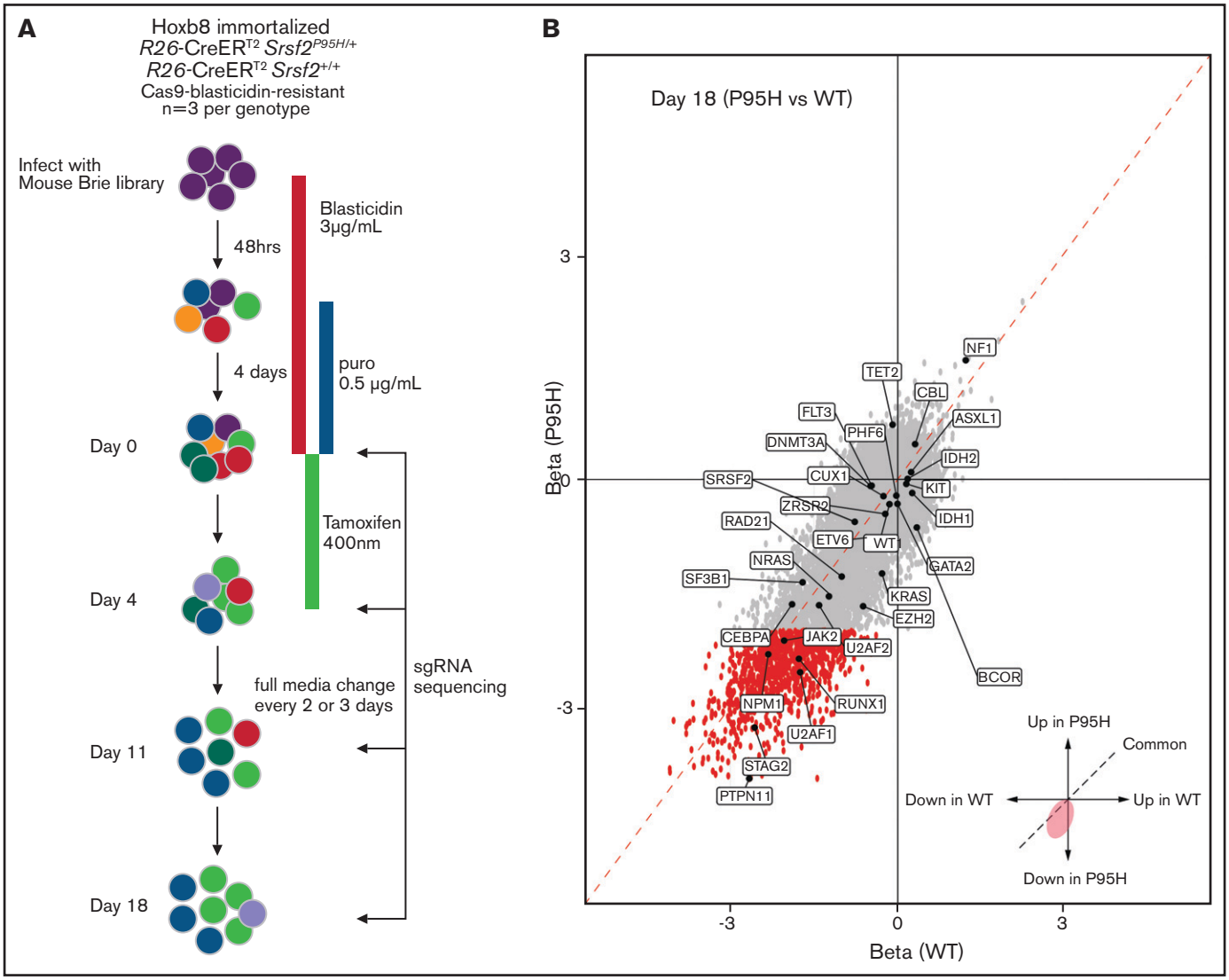

Figure 3. Genome-wide CRISPR knock-out *Srsf2*$^{P95H/+}$ screen. (A) Schematic outline of the pooled CRISPR knock-out *Srsf2* screen. (B) Visualization of performance of sgRNA against genes mutated in MDS and MDS/myeloproliferative neoplasm at day 18 of the screen. Gray dots, all the sgRNA identified; red dots, sgRNA with FDR $<$ .01 and β score <-2.

between Cas9 *Srsf2*$^{P95H/+}$ and Cas9 *Srsf2*$^{+/+}$ cells also decreased, indicating mutant and WT cells responded differently to the pooled genome knockout (supplemental Table 4). We next assessed the depletion of essential genes from the samples in the screen. Using the Cluster of the Essential Gene (CEG2) database, we annotated and visualized the negative selection of essential genes using MaGeCK maximum likelihood estimation (supplemental Table 5).[23,40] At day 4, essential genes were equally depleted from *Srsf2*$^{P95H/+}$ and *Srsf2*$^{+/+}$ cells. Genes from the essential ribosome pathways, such as *Rps15A*, *Rps7*, *Rpl23*, *Rplp2*, *Rps8,* and *Rpl8*, were among the most depleted genes in the screen. In addition, cell line-specific essential genes such as *Hoxb8* and *Csf2ra* (indicated in green), were depleted in both genotypes. Both *Hoxb8* and *Csf2ra* (GM-CSF receptor) would be expected to be lost because the cell lines are immortalized with Hoxb8 and dependent on GM-CSF for survival and proliferation.

We then assessed the performance of sgRNA against genes that are recurrently mutated in human MDS and related myeloid neoplasms (Figure 3B). At day 18, multiple spliceosome genes, such as *Srsf2*, *Sf3b1*, *U2af1*, *U2af2,* and *Zrsr2* were all negatively selected in both *Srsf2*$^{P95H/+}$ and *Srsf2*$^{+/+}$ cells. This is expected because complete loss of key spliceosome genes resulted in cell death or embryonic lethality in murine models.[34,41] Looking at genes of which loss of function is known to be cooperative with *SRSF2*^{P95H} mutation, sgRNA targeting *Tet2* (FDR = 0.05), or *Cbl* (FDR = 0.02) showed a positive enrichment in *Srsf2*$^{P95H/+}$ cells. This is consistent with the human genetics where *TET2* loss-of-function mutations frequently cooccur with *SRSF2* mutation.[42] A caveat with this analysis is that genes with recurrent truncating or point mutations are unlikely to be captured with this approach because Cas9 cleavage results in indels and therefore most likely gene disruption near the target sites.

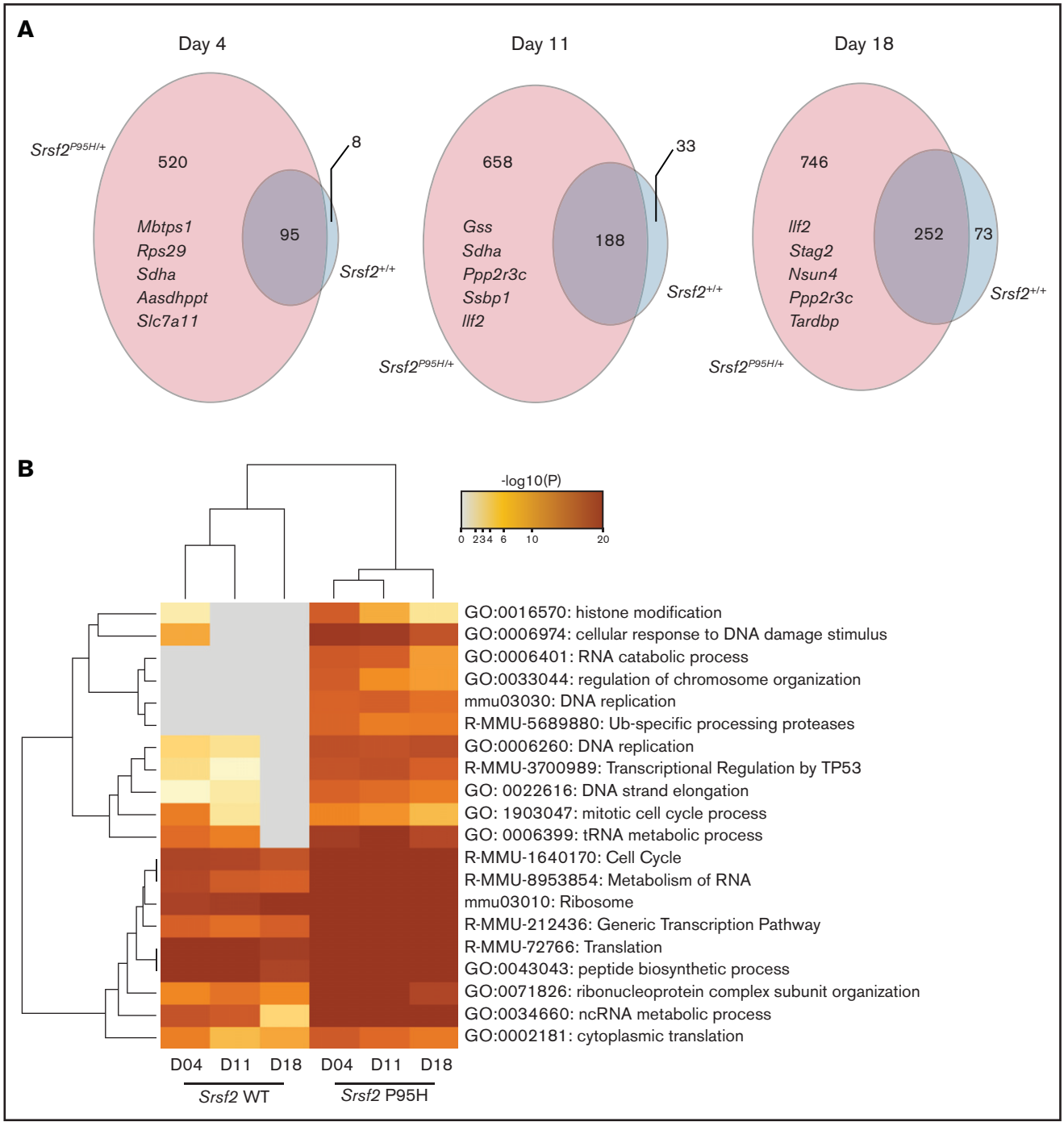

Figure 4. DNA replication, cell-cycle, and DNA damage response are among the top negatively selected pathways in screen. (A) The number of genes negatively selected at days 4, 11, and 18 in *Srsf2*$^{P95H/+}$ (pink) and *Srsf2*$^{+/+}$ (blue) cells. The top 5 negatively selected genes for *Srsf2*$^{P95H/+}$ cells ranked by β score of all 3 cell lines at each timepoint are listed. FDR < 0.01, β score < -1, and any CEG2 essential genes are excluded. (B) Pathway analysis of the negatively selected genes for *Srsf2*$^{+/+}$ and *Srsf2*$^{P95H/+}$ at 3 timepoints showing DNA replication, cell-cycle, and DNA damage response pathways have a more negative effect on *Srsf2*$^{P95H/+}$ cell survival when perturbed.

Pooled CRISPR knock-out screen reveals genetic vulnerabilities of *Srsf2* mutant cells in cell-cycle and DNA repair pathways

To determine candidate genes that are negatively selected in Cas9 *Srsf2*$^{P95H/+}$ compared with the Cas9 *Srsf2*$^{+/+}$ cells, we set inclusion criteria as FDR < 0.01, β score < -1, no CEG2 essential genes, and the number of sgRNA recovered ≥ 3. The β score represents the degree and direction a gene is selected. Overall, the number of negatively selected sgRNA was higher in the *Srsf2*$^{P95H/+}$ cells than in the *Srsf2*$^{+/+}$ cells (Figure 4A). At each time point, the majority of genes depleted in the WT cells overlapped with the

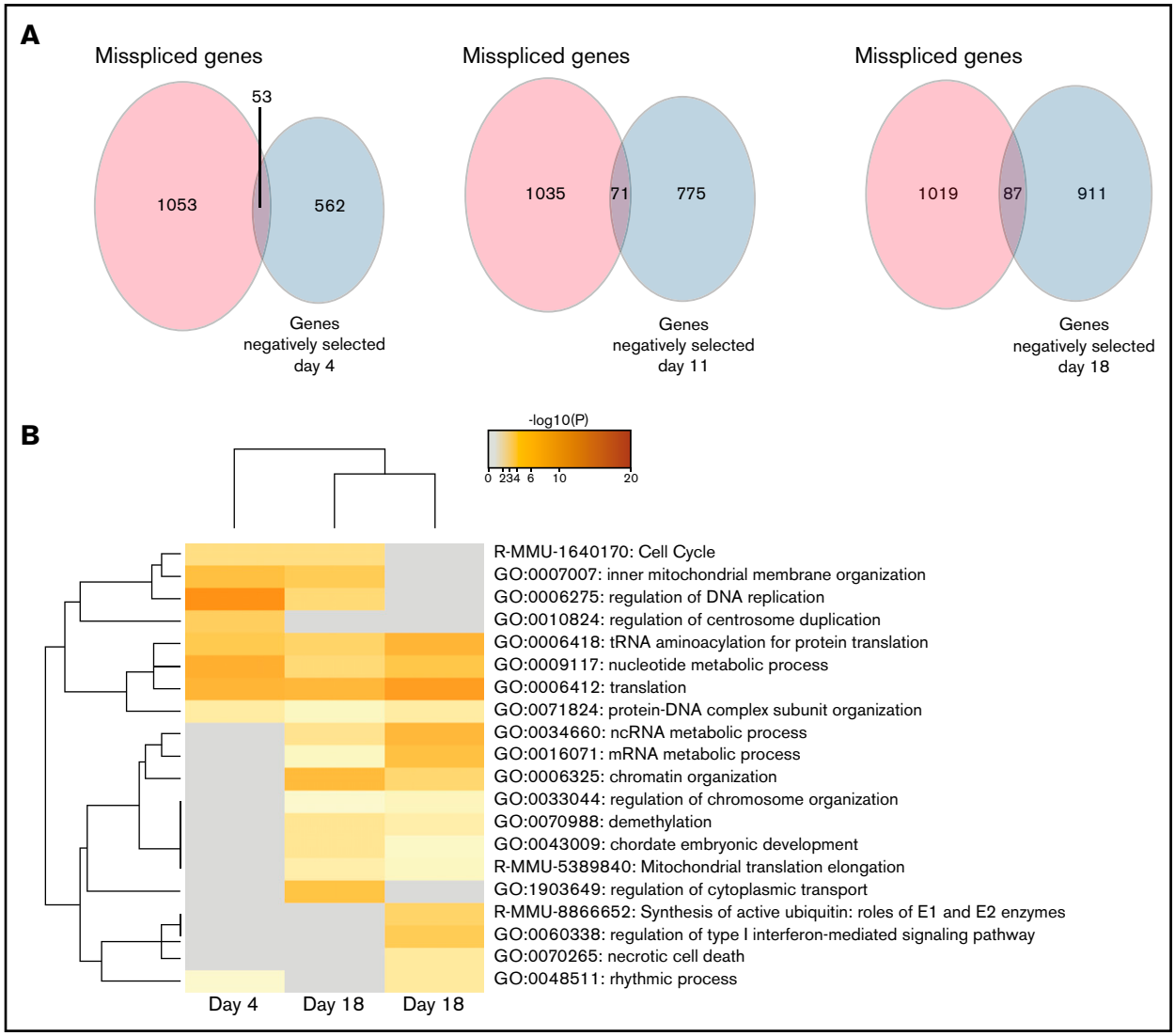

Figure 5. Genes from the cell-cycle and regulation of DNA replication pathways are both misspliced and negatively selected in *Srsf2*$^{P95H/+}$ cells. (A) Venn diagrams showing the overlap between the genes that are misspliced in the GM-CSF *Srsf2*$^{P95H/+}$ cells and the genes that are negatively selected at days 4, 11, and 18 of the *Srsf2* CRISPR screen. (B) Pathway analysis showing that genes associated with cell-cycle and DNA replication regulation are misspliced and cause cell death when deleted in *Srsf2*$^{P95H/+}$ cells.

genes depleted in the P95H cells. This suggested that WT cells share most of their genetic sensitivities with *Srsf2*$^{P95H/+}$ cells, whereas mutant cells are sensitive to an additional set of genetic perturbations. We then performed analysis of the genes and pathways negatively selected in *Srsf2*$^{P95H/+}$ and *Srsf2*$^{+/+}$ cells using Metascape.[25] The top 20 most significant pathways are listed in Figure 4B. From the analysis, sgRNA within the RNA metabolism, ribosome, and translation pathways were significantly depleted in both P95H and WT cells, although they tended to be more significantly depleted in P95H cells. Interestingly, there were a number of pathways that were specific to the P95H cells or also present in the WT cells but at a much lower level of significance. These pathways include histone modification/chromosome organization, DNA damage response/DNA repair, and cell-cycle pathways. The results indicate that potential genetic vulnerabilities of *Srsf2*$^{P95H/+}$ cells are contained within these pathways.

Misspliced genes in cell-cycle pathways are essential for *Srsf2*$^{P95H/+}$ cells survival

After determining the negatively selected sgRNAs in Cas9 *Srsf2*$^{P95H/+}$ cells, we tested if any of the genes were contained within the differentially spliced transcripts of the *Srsf2*$^{P95H/+}$ cells. Aberrant transcripts generated by missplicing could potentially lead to changes in protein function and promote cell survival and proliferation of the mutant cells. Knock-out of the genes, as undertaken in the screen, could prevent these aberrant transcripts arising and therefore cause cell death. We searched for overlap between the misspliced transcripts generated from Cas9 *Srsf2*$^{P95H/+}$ cells at day 11 (Figure 1) and the negatively selected genes during the whole course of the screen. Upon comparison, there was little overlap (less than 10%) between the 2 datasets (Figure 5A). Among the overlapping genes, *Npm1*, *Dap3,* and *Runx1* were identified at all the timepoints, whereas *Hnrnpa2b1* was only identified at day

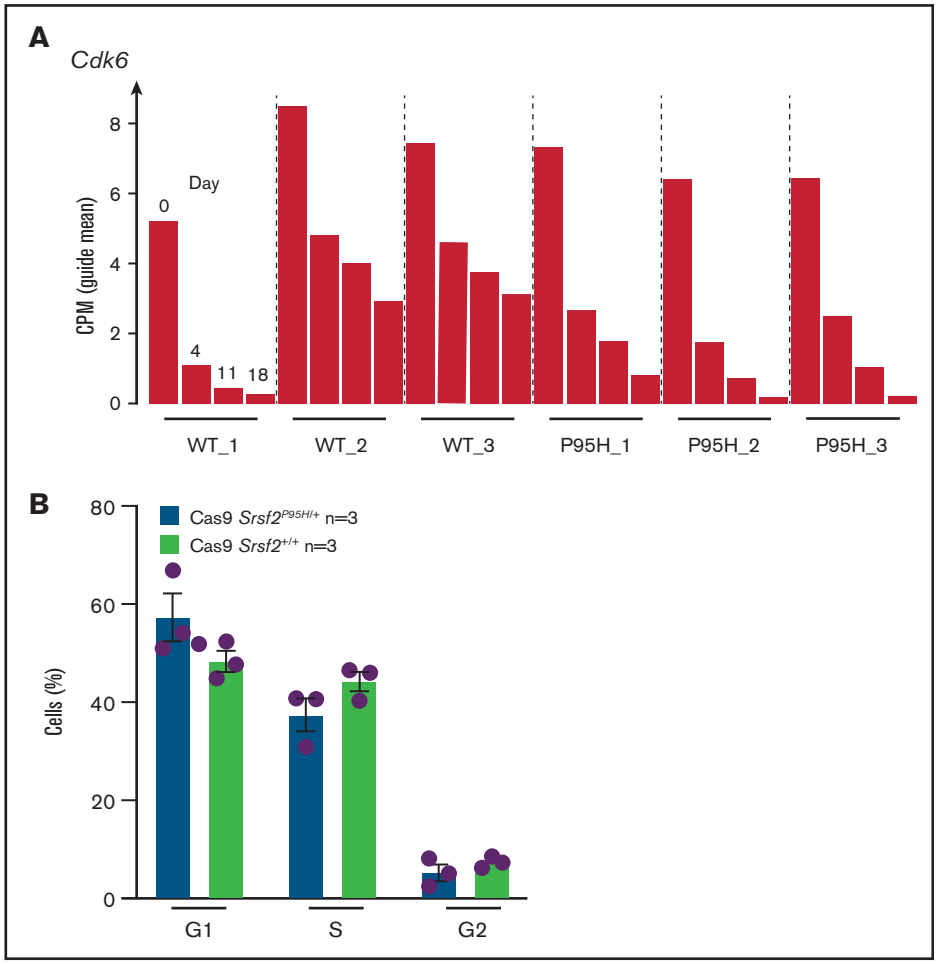

Figure 6. *Srsf2*$^{P95H/+}$ cells are sensitive to the CDK6 inhibitor palbociclib and the spliceosome inhibitor Pladienolide B. (A) The guide count for CDK6 sgRNA in *Srsf2*$^{+/+}$ and *Srsf2*$^{P95H/+}$ cells over the course of the screen. (B) The cell-cycle stage distribution of *Srsf2*$^{P95H/+}$ and *Srsf2*$^{+/+}$ cells at day 18 after tamoxifen cessation. No statistical difference detected between P95H and WT cells. (C) Hoxb8 GM-CSF *Srsf2*$^{P95H/+}$ cell lines and sorted primary *Srsf2*$^{P95H/+}$ LKS^{+} cells are sensitive to palbociclib and Pladienolide B after 4 days of drug culture. Hoxb8 GM-CSF cell lines: n = 3 per genotype for roscovitine and Pladienolide B, n = 2 for palbociclib. Extra sum-of-squares F test. LKS^{+} cells, n = 1 per genotype. LKS^{+}, lin^{-}ckit^{+}Sca-1^{+}.

18. Interestingly, genes belonging to the cell-cycle pathway were identified as both misspliced and negatively selected in *Srsf2*$^{P95H/+}$ cells (Figure 5B). Other pathways found in the negatively selected list, such as translation, RNA metabolism, and chromosome organization were also pathways enriched in misspliced transcripts in *Srsf2*$^{P95H/+}$ cells. Together, the data suggest that these pathways have a close genetic interaction with *Srsf2*$^{P95H/+}$, especially the cell-cycle pathways.

Palbociclib, a CDK6 inhibitor, preferentially inhibits *Srsf2*$^{P95H/+}$ cell growth

After analyzing the functional relationships of the negatively selected genes, we searched for druggable targets by comparing the negatively selected genes at day 18 with the Drug-Gene Interaction database.[43-45] Selected candidates were further tested using in vitro dose response assays to validate the synthetic lethality. The cell cycle–related gene *Cdk6*, among the top 30 negatively selected genes at day 18 using MaGeCK[24] analysis (supplemental Figure 6A), was prioritized as a druggable target. Evaluation of the *Cdk6* sgRNA from the screen indicated that there was a substantial drop in the number of guides in all 3 Cas9 *Srsf2*$^{P95H/+}$ cell lines, whereas significantly less depletion was observed in 2 of the 3 Cas9 *Srsf2*$^{+/+}$ cell lines (Figure 6A). Subsequent analysis of the cell lines showed no inherent differences between the cell-cycle profiles of *Srsf2*$^{P95H/+}$ and WT cells (Figure 6B). We then tested the sensitivity of the cell lines (n = 3 per genotype) to inhibition of CDK6 using palbociclib. Roscovitine which is a CDK2/5 inhibitor was used as a negative control because we did not find depletion of *Cdk2* sgRNA from the P95H cells (supplemental Figure 6B). We also tested Pladienolide B, a spliceosome inhibitor, as a positive control (Figure 6C, top). The results showed that *Srsf2*$^{P95H/+}$ cells had a near threefold reduction in the IC_{50} value of palbociclib ($P < .0001$, extra sum-of-squares F test), compared with *Srsf2*$^{+/+}$ cells. Consistent with the screen results, roscovitine did not show any specific inhibition of *Srsf2*$^{P95H/+}$ cells, whereas Pladienolide B was approximately twofold more toxic to *Srsf2*$^{P95H/+}$ cells than WT cells, which is in agreement with previous reports.[10,18] In addition to *Cdk6*, we performed drug assay using tigecycline[46] and murbritinib[47] because several mitochondrial respiratory genes including *Uqcrc1*, *Cox6b1*, *Atp5a1,* and *Uqcc2* were among the top 30 negatively selected genes in *Srsf2* mutant cells

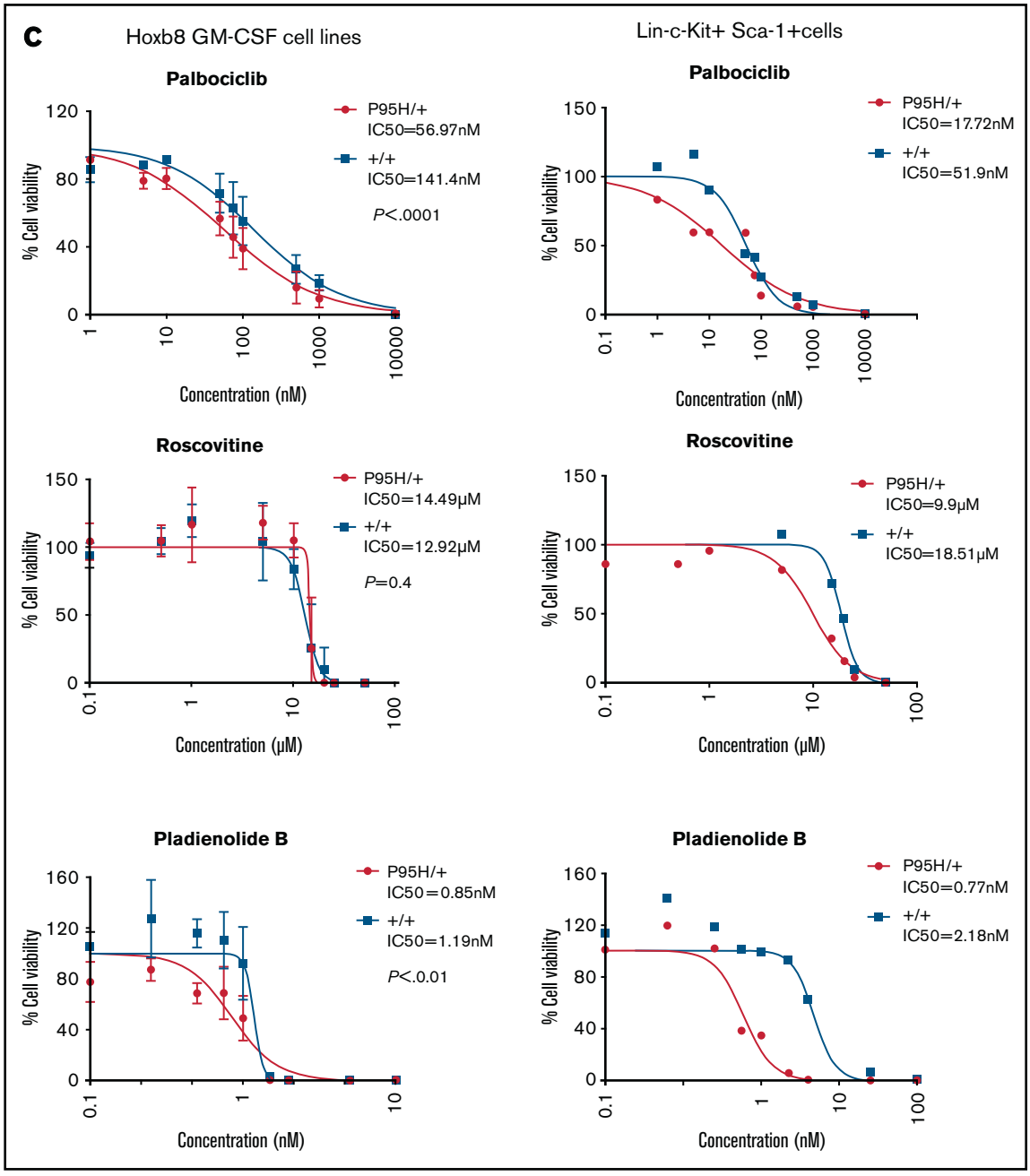

Figure 6. (continued)

(supplemental Figure 6A). However, both drugs showed no effect in targeting *Srsf2* mutant cells (supplemental Figure 6D).

We then tested palbociclib on primary *Srsf2*$^{P95H/+}$ cells. LKS^{+} cells were sorted from *R26*-CreERT2$^{ki/+}$ *Srsf2*$^{+/+}$ and *R26*-CreERT2$^{ki/+}$ *Srsf2*$^{P95H/+}$ mice, tamoxifen treated in vitro before coculturing with palbociclib, roscovitine, and Pladienolide B for 4 days (Figure 6C, bottom). The results showed that primary *Srsf2*$^{P95H/+}$ cells had a threefold reduction in the IC_{50} value of palbociclib as well as Pladienolide B. Roscovitine showed a twofold difference between *Srsf2*$^{P95H/+}$ and *Srsf2*$^{+/+}$ cells. Taken together, the results demonstrate that palbociclib displays a preferential inhibition of *Srsf2*$^{P95H/+}$ cells in both Hoxb8 immortalized cell lines and in primary LKS^{+} cells.

Discussion

Despite recent efforts to identify means of targeting splicing-mutant myeloid neoplasms and leukemia, targeting of the remaining WT splicing apparatus has proven toxic and with a limited therapeutic window.[7,12,18,48] By comparing multiple human and murine datasets, we identified cell cycle, DNA repair, and chromatin organization and modification as overrepresented pathways within the misspliced transcripts of both human and mouse *Srsf2*$^{P95H/+}$ cells. RNA-seq analysis of Cas9 *Srsf2*$^{P95H/+}$ cells, a cell model generated to exclude confounding mutations often detected in existing cell lines, showed similar missplicing changes compared with the in vivo model. Using these Cas9 cells, we performed a functional screen to

experimentally determine genetic sensitivities of *Srsf2*$^{P95H/+}$ mutation. With 3 biological replicates per group, we discovered that cell-cycle and DNA damage response pathways are coessential with *Srsf2*$^{P95H/+}$ mutation.

It is unknown whether the genetic interaction we observed is an SRSF2 mutant-specific phenomena or if it would apply to other recurrent splicing mutations such as *SF3B1*^{K700E} and *U2AF1*^{S34}. Previously, it has been demonstrated that RNA splicing and cell cycle are interconnected. Adequate splicing of cell-cycle genes, such as *CDC25* and *CDK2*, are required for a proper transition between different cell-cycle phases[49,50] and disruption of core spliceosome components, such as deletion of SRSF2, leads to G2-phase cell-cycle arrest and apoptosis.[51-53] It is possible that mutant splicing factors diminish the capacity of the spliceosome, which is critical for normal cell-cycle progression, and that mutant cells heavily rely on the remaining WT allele for survival. This is supported by the observation that no homozygous (*Srsf2*$^{P95H/P95H}$) or hemizygous (*Srsf2*$^{P95H/-}$) mutations have been reported in human cancers. Our analysis indicates that splicing mutant cells are unable to cope with further disruption of cell-cycle pathways that indirectly results in cell death. It is also possible that disruption of the cell cycle has a more direct impact on RNA splicing. A recent study by Rimel et al reports that inhibition of cell-cycle regulator CDK7 could lead to widespread splicing defects.[54] This is similar to the effect of spliceosome inhibition and may at least partly be responsible for the synergistic interaction that we observed.

Through our analysis of negatively selected genes and the direct testing of genetic interactions, we were able to identify CDK6, a cell-cycle regulator, as a potential new therapeutic target for *Srsf2*$^{P95H/+}$ mutation. Pharmacological inhibition of CDK6 with palbociclib resulted in a threefold reduction in IC_{50} in both *Srsf2*$^{P95H/+}$ cell lines and primary *Srsf2*$^{P95H/+}$ cells, compared with the respective WT cells. Although palbociclib is also a potent inhibitor of CDK4, unlike *Cdk6* sgRNA, *Cdk4* sgRNA was not preferentially depleted in the P95H cells (supplemental Figure 6C). The inhibitory effect of palbociclib on P95H cell growth is thus likely because of CDK6 inhibition. This is the first report that a cell-cycle inhibitor could be used to target splicing mutant cells. In normal HSCs, CDK6 is associated with the regulation of hematopoietic stem cell quiescence.[55,56] In MLL-AF9 leukemic cell lines, inhibition of CDK6 has been shown to attenuate the growth and to overcome the block to myeloid differentiation.[57,58] In breast cancer patients,[59] however, neutropenia is a known side effect of palbociclib treatment. It is possible that in vivo palbociclib inhibits excessive proliferation of myeloid population. Because this is a key phenotypic feature of *SRSF2*$^{P95H/+}$ mutation,[4,5,18] this could be an advantage in the treatment of SRSF2 mutant MDS. Exactly how inhibition of CDK6 induces lethality in our *Srsf2*$^{P95H/+}$ cells is unclear. Nevertheless, the functional and pharmacological investigation demonstrates a close genetic interaction between cell-cycle regulation pathways and *Srsf2*$^{P95H/+}$ mutation.

Besides cell cycle, the DNA damage response pathway was also identified as a genetic interactor with *Srsf2*$^{P95H/+}$ mutation. Aberrant RNA splicing has been reported to lead to genome instability via increased *R*-loop formation and possible suboptimal splicing of key transcripts for genome maintenance.[60] On 1 hand, impairment of the splicing machinery, such as depletion of SRSF2 and SRSF2^{P95H} mutation, may lead to accumulation of *R*-loops, which is linked with replication folk stalling and DNA replication stress.[61,62] On the other hand, key response elements of DNA repair, such as ATR, are misspliced in *Srsf2*$^{P95H/+}$ mutant cells. It is possible that 1 or both of these factors may contribute to the synthetic lethality observed with the inhibition of the DNA damage response pathway. Additional investigations may expose more intrinsic vulnerabilities of splicing factor mutant cells and decipher how splicing mutation induced DNA damage may contribute to cancer development.

Overall, we have identified that the cell-cycle and DNA damage response are overrepresented within the recurrently misspliced transcripts of SRSF2$^{P95H/+}$ across both human and mouse samples. Using agnostic genome-wide screening, we demonstrate that targeting of these pathways in combination with *Srsf2*$^{P95H/+}$ mutation reveals a previously unrecognized vulnerability to CDK6 inhibition by palbociclib. Therefore, our study identifies a close genetic relationship between the cell-cycle and DNA damage response/DNA repair pathway with *Srsf2*$^{P95H/+}$ mutation and a new therapeutic opportunity outside of spliceosome inhibition.

Acknowledgments

The authors thank J. Heierhorst, L. Purton, J. Heraud-Farlow, J. Pimanda, A. Unnikrishnan, K.P. Truong, and M. Pillai for comments and discussion; S. Taylor for technical assistance; St. Vincent's Hospital BioResources Centre for care of experimental animals; St. Vincent's Institute Flow Cytometry Core Facility; M Kamps for HoxB8 plasmids; Addgene for plasmid distribution; and Novogene for DNA and A sequencing.

This work was supported by the Cancer Council of Victoria (C.R.W., A.M.C., APP1126010), Victorian Cancer Agency Research Fellowship (C.R.W., MCRF15015), and in part by the Victorian State Government OIS to St Vincent's Institute. The Victorian Centre for Functional Genomics (K.J.S.) is funded by the Australian Cancer Research Foundation, Phenomics Australia through funding from the Australian Government's National Collaborative Research Infrastructure Strategy program, and the Peter MacCallum Cancer Centre Foundation.

Authorship

Contribution: J.J.X., M.F.S., and C.R.W. conceptualized the study; J.J.X., M.F.S., I.N., K.J.S., and C.R.W. designed the experiments; J.J.X., M.F.S., and A.M.C. performed the experiments; J.J.X. and A.M.C. produced the figures; J.J.X. wrote the original manuscript; J.J.X., M.F.S., A.M.C., and C.R.W. reviewed and edited the manuscript; A.M.C. and C.R.W. were responsible for funding acquisition; I.N. and K.J.S. provided resources; and M.F.S., K.J.S., and C.R.W. provided supervision.

Conflict-of-interest disclosure: The authors declare no competing financial interests.

ORCID profiles: A.M.C., 0000-0002-9630-6236; K.J.S., 0000-0001-9136-1781; M.F.S., 0000-0001-6027-4108; C.R.W., 0000-0002-4784-9031

Correspondence: Carl Walkley, St Vincent's Institute, 9 Princes St, Fitzroy 3065 VIC, Australia; e-mail: cwalkley@svi.edu.au; and Monique Smeets, St Vincent's Institute, 9 Princes St, Fitzroy 3065 VIC, Australia; e-mail: msmeets@svi.edu.au.

References

1. Yoshida K, Sanada M, Shiraishi Y, et al. Frequent pathway mutations of splicing machinery in myelodysplasia. *Nature.* 2011;478(7367):64-69.
2. Anczuków O, Krainer AR. Splicing-factor alterations in cancers. *RNA.* 2016;22(9):1285-1301.
3. Zhang J, Lieu YK, Ali AM, et al. Disease-associated mutation in SRSF2 misregulates splicing by altering RNA-binding affinities. *Proc Natl Acad Sci USA.* 2015;112(34):E4726-E4734.
4. Kim E, Ilagan JO, Liang Y, et al. SRSF2 mutations contribute to myelodysplasia by mutant-specific effects on exon recognition. *Cancer Cell.* 2015; 27(5):617-630.
5. Kon A, Yamazaki S, Nannya Y, et al. Physiological *Srsf2* P95H expression causes impaired hematopoietic stem cell functions and aberrant RNA splicing in mice. *Blood.* 2018;131(6):621-635.
6. Bonnal S, Vigevani L, Valcárcel J. The spliceosome as a target of novel antitumour drugs. *Nat Rev Drug Discov.* 2012;11(11):847-859.
7. Lee SC, Abdel-Wahab O. Therapeutic targeting of splicing in cancer. *Nat Med.* 2016;22(9):976-986.
8. Pangallo J, Kiladjian JJ, Cassinat B, et al. Rare and private spliceosomal gene mutations drive partial, complete, and dual phenocopies of hotspot alterations. *Blood.* 2020;135(13):1032-1043.
9. Kaida D, Motoyoshi H, Tashiro E, et al. Spliceostatin A targets SF3b and inhibits both splicing and nuclear retention of pre-mRNA. *Nat Chem Biol.* 2007;3(9):576-583.
10. Kotake Y, Sagane K, Owa T, et al. Splicing factor SF3b as a target of the antitumor natural product pladienolide. *Nat Chem Biol.* 2007;3(9): 570-575.
11. Seiler M, Yoshimi A, Darman R, et al. H3B-8800, an orally available small-molecule splicing modulator, induces lethality in spliceosome-mutant cancers. *Nat Med.* 2018;24(4):497-504.
12. Hong DS, Kurzrock R, Naing A, et al. A phase I, open-label, single-arm, dose-escalation study of E7107, a precursor messenger ribonucleic acid (pre-mRNA) splicesome inhibitor administered intravenously on days 1 and 8 every 21 days to patients with solid tumors. *Invest New Drugs.* 2014; 32(3):436-444.
13. Platzbecker U, Yu K, Yuan X, et al. Results of a clinical trial of H3B-8800, a splicing modulator, in patients with myelodysplastic syndromes (MDS), acute myeloid leukemia (AML) or chronic myelomonocytic leukemia (CMML). *Blood.* 2019;134(suppl 1):673.
14. Bryant HE, Schultz N, Thomas HD, et al. Specific killing of BRCA2-deficient tumours with inhibitors of poly(ADP-ribose) polymerase [published correction appears in *Nature.* 2007;447(7142):346]. *Nature.* 2005;434(7035):913-917.
15. Dhanjal JK, Radhakrishnan N, Sundar D. Identifying synthetic lethal targets using CRISPR/Cas9 system. *Methods.* 2017;131:66-73.
16. Wang T, Yu H, Hughes NW, et al. Gene essentiality profiling reveals gene networks and synthetic lethal interactions with oncogenic Ras. *Cell.* 2017;168(5):890-903.e15.
17. O'Neil NJ, Bailey ML, Hieter P. Synthetic lethality and cancer. *Nat Rev Genet.* 2017;18(10):613-623.
18. Smeets MF, Tan SY, Xu JJ, et al. *Srsf2 P95H* initiates myeloid bias and myelodysplastic/myeloproliferative syndrome from hemopoietic stem cells. *Blood.* 2018;132(6):608-621.
19. Xu JJ, Smeets MF, Tan SY, Wall M, Purton LE, Walkley CR. Modeling human RNA spliceosome mutations in the mouse: not all mice were created equal. *Exp Hematol.* 2019;70:10-23.
20. Wang GG, Calvo KR, Pasillas MP, Sykes DB, Häcker H, Kamps MP. Quantitative production of macrophages or neutrophils ex vivo using conditional Hoxb8. *Nat Methods.* 2006;3(4):287-293.
21. Sanjana NE, Shalem O, Zhang F. Improved vectors and genome-wide libraries for CRISPR screening. *Nat Methods.* 2014;11(8):783-784.
22. Jeong HH, Kim SY, Rousseaux MWC, Zoghbi HY, Liu Z. Beta-binomial modeling of CRISPR pooled screen data identifies target genes with greater sensitivity and fewer false negatives. *Genome Res.* 2019;29(6):999-1008.
23. Li W, Köster J, Xu H, et al. Quality control, modeling, and visualization of CRISPR screens with MAGeCK-VISPR. *Genome Biol.* 2015;16(1):281.
24. Li W, Xu H, Xiao T, et al. MAGeCK enables robust identification of essential genes from genome-scale CRISPR/Cas9 knockout screens. *Genome Biol.* 2014;15(12):554.
25. Zhou Y, Zhou B, Pache L, et al. Metascape provides a biologist-oriented resource for the analysis of systems-level datasets. *Nat Commun.* 2019; 10(1):1523.
26. Chalk AM, Taylor S, Heraud-Farlow JE, Walkley CR. The majority of A-to-I RNA editing is not required for mammalian homeostasis. *Genome Biol.* 2019;20(1):268.
27. Heraud-Farlow JE, Chalk AM, Linder SE, et al. Protein recoding by ADAR1-mediated RNA editing is not essential for normal development and homeostasis. *Genome Biol.* 2017;18(1):166.
28. Love MI, Huber W, Anders S. Moderated estimation of fold change and dispersion for RNA-seq data with DESeq2. *Genome Biol.* 2014;15(12): 550.
29. Lin KT, Krainer AR. PSI-Sigma: a comprehensive splicing-detection method for short-read and long-read RNA-seq analysis. *Bioinformatics.* 2019; 35(23):5048-5054.

30. Garrido-Martín D, Palumbo E, Guigó R, Breschi A. ggsashimi: Sashimi plot revised for browser- and annotation-independent splicing visualization. *PLOS Comput Biol.* 2018;14(8):e1006360.

31. Shen S, Park JW, Lu ZX, et al. rMATS: robust and flexible detection of differential alternative splicing from replicate RNA-Seq data. *Proc Natl Acad Sci USA.* 2014;111(51):E5593-E5601.

32. Hershberger CE, Moyer DC, Adema V, et al. Complex landscape of alternative splicing in myeloid neoplasms. *Leukemia.* 2021;35(4):1108-1120.

33. Yoshimi A, Lin KT, Wiseman DH, et al. Coordinated alterations in RNA splicing and epigenetic regulation drive leukaemogenesis. *Nature.* 2019; 574(7777):273-277.

34. Komeno Y, Huang YJ, Qiu J, et al. SRSF2 is essential for hematopoiesis, and its myelodysplastic syndrome-related mutations dysregulate alternative pre-mRNA splicing. *Mol Cell Biol.* 2015;35(17):3071-3082.

35. Qiu J, Zhou B, Thol F, et al. Distinct splicing signatures affect converged pathways in myelodysplastic syndrome patients carrying mutations in different splicing regulators. *RNA.* 2016;22(10):1535-1549.

36. Hurtado AM, Luengo-Gil G, Chen-Liang TH, et al. Transcriptomic rationale for synthetic lethality-targeting ERCC1 and CDKN1A in chronic myelomonocytic leukaemia. *Br J Haematol.* 2018;182(3):373-383.

37. Bhoumik A, Takahashi S, Breitweiser W, Shiloh Y, Jones N, Ronai Z. ATM-dependent phosphorylation of ATF2 is required for the DNA damage response. *Mol Cell.* 2005;18(5):577-587.

38. Shimizu M, Nomura Y, Suzuki H, et al. Activation of the rat cyclin A promoter by ATF2 and Jun family members and its suppression by ATF4. *Exp Cell Res.* 1998;239(1):93-103.

39. Doench JG, Fusi N, Sullender M, et al. Optimized sgRNA design to maximize activity and minimize off-target effects of CRISPR-Cas9. *Nat Biotechnol.* 2016;34(2):184-191.

40. Hart T, Tong AHY, Chan K, et al. Evaluation and design of genome-wide CRISPR/SpCas9 knockout screens. *G3 (Bethesda).* 2017;7(8): 2719-2727.

41. Isono K, Mizutani-Koseki Y, Komori T, Schmidt-Zachmann MS, Koseki H. Mammalian polycomb-mediated repression of Hox genes requires the essential spliceosomal protein Sf3b1. *Genes Dev.* 2005;19(5):536-541.

42. Ogawa S. Genetics of MDS. *Blood.* 2019;133(10):1049-1059.

43. Cotto KC, Wagner AH, Feng YY, et al. DGIdb 3.0: a redesign and expansion of the drug-gene interaction database. *Nucleic Acids Res.* 2018;46(D1): D1068-D1073.

44. Griffith M, Griffith OL, Coffman AC, et al. DGIdb: mining the druggable genome. *Nat Methods.* 2013;10(12):1209-1210.

45. Wagner AH, Coffman AC, Ainscough BJ, et al. DGIdb 2.0: mining clinically relevant drug-gene interactions. *Nucleic Acids Res.* 2016;44(D1): D1036-D1044.

46. Skrtić M, Sriskanthadevan S, Jhas B, et al. Inhibition of mitochondrial translation as a therapeutic strategy for human acute myeloid leukemia. *Cancer Cell.* 2011;20(5):674-688.

47. Baccelli I, Gareau Y, Lehnertz B, et al. Mubritinib targets the electron transport chain complex I and reveals the landscape of OXPHOS dependency in acute myeloid leukemia. *Cancer Cell.* 2019;36(1):84-99.e8.

48. Obeng EA, Chappell RJ, Seiler M, et al. Physiologic expression of Sf3b1(K700E) causes impaired erythropoiesis, aberrant splicing, and sensitivity to therapeutic spliceosome modulation. *Cancer Cell.* 2016;30(3):404-417.

49. Albert H, Battaglia E, Monteiro C, Bagrel D. Genotoxic stress modulates CDC25C phosphatase alternative splicing in human breast cancer cell lines. *Mol Oncol.* 2012;6(5):542-552.

50. Ji X, Humenik J, Yang D, Liebhaber SA. PolyC-binding proteins enhance expression of the CDK2 cell cycle regulatory protein via alternative splicing. *Nucleic Acids Res.* 2018;46(4):2030-2044.

51. Ahn EY, DeKelver RC, Lo MC, et al. SON controls cell-cycle progression by coordinated regulation of RNA splicing. *Mol Cell.* 2011;42(2): 185-198.

52. Shin C, Manley JL. The SR protein SRp38 represses splicing in M phase cells. *Cell.* 2002;111(3):407-417.

53. Li X, Wang J, Manley JL. Loss of splicing factor ASF/SF2 induces G2 cell cycle arrest and apoptosis, but inhibits internucleosomal DNA fragmentation. *Genes Dev.* 2005;19(22):2705-2714.

54. Rimel JK, Poss ZC, Erickson B, et al. Selective inhibition of CDK7 reveals high-confidence targets and new models for TFIIH function in transcription. *Genes Dev.* 2020;34(21-22):1452-1473.

55. Laurenti E, Frelin C, Xie S, et al. CDK6 levels regulate quiescence exit in human hematopoietic stem cells. *Cell Stem Cell.* 2015;16(3):302-313.

56. Scheicher R, Hoelbl-Kovacic A, Bellutti F, et al. CDK6 as a key regulator of hematopoietic and leukemic stem cell activation [published correction appears in *Blood*. 2015;125(1):90–101]. *Blood.* 2015;125(1):90-101.

57. Fujimoto T, Anderson K, Jacobsen SE, Nishikawa SI, Nerlov C. Cdk6 blocks myeloid differentiation by interfering with Runx1 DNA binding and Runx1-C/EBPalpha interaction. *EMBO J.* 2007;26(9):2361-2370.

58. Placke T, Faber K, Nonami A, et al. Requirement for CDK6 in MLL-rearranged acute myeloid leukemia. *Blood.* 2014;124(1):13-23.

59. Finn RS, Martin M, Rugo HS, et al. Palbociclib and letrozole in advanced breast cancer. *N Engl J Med.* 2016;375(20):1925-1936.

60. Helmrich A, Ballarino M, Nudler E, Tora L. Transcription-replication encounters, consequences and genomic instability. *Nat Struct Mol Biol.* 2013; 20(4):412-418.

61. Li X, Manley JL. Inactivation of the SR protein splicing factor ASF/SF2 results in genomic instability. *Cell.* 2005;122(3):365-378.

62. Chen L, Chen JY, Huang YJ, et al. The augmented R-loop is a unifying mechanism for myelodysplastic syndromes induced by high-risk splicing factor mutations. *Mol Cell.* 2018;69(3):412-425.e6.